Nanoscale Advances

ROYAL SOCIETY OF CHEMISTRY

PAPER

View Article Online
View Journal | View Issue

Cite this: *Nanoscale Adv.*, 2021, **3**, 5068

Ultrafine Ru nanoclusters supported on N/S doped macroporous carbon spheres for efficient hydrogen evolution reaction†

Yijie Wang, Wenjie Luo, Haojie Li and Chuanwei Cheng *

The construction of highly-active and stable electrocatalysts for the hydrogen evolution reaction (HER) is significant for efficient water splitting processes. Herein, we develop an efficient HER catalyst of ultrafine Ru nanoclusters supported on a N/S doped macroporous hollow carbon sphere (Ru/H–S,N–C). The N/S co-doping strategy not only facilitates the reduction of the Ru nanocluster sizes, but also regulates the electronic structure of metallic Ru, improving the HER activity of the metallic Ru catalyst. Due to the structural advantages of N/S-doped macroporous carbon spheres that provide a fast mass transfer process and the high intrinsic activity of Ru nanoclusters, the optimized Ru/H–S,N–C catalyst exhibits excellent HER performance in alkaline medium, with a low overpotential of 32 mV to reach 10 mA cm^{-2}, fast HER kinetics (a Tafel slope of 24 mV dec^{-1}) and excellent durability, superior to the performances of the Ru/H–N–C sample and commercial Pt/C catalyst. Our work offers some guidance on the design of efficient Ru-based electrocatalysts.

Received 6th June 2021
Accepted 22nd July 2021

DOI: 10.1039/d1na00424g

rsc.li/nanoscale-advances

1. Introduction

Hydrogen (H_2), with its advantages of high gravimetric energy density, sustainability, and environmental friendliness,[1–3] is considered a promising alternative to traditional fossil fuels. Among the various approaches for hydrogen production, water electrolysis is an ideal method, with zero carbon emission, abundant water resources, and high purity.[4,5] However, the lack of efficient electrocatalysts to lower the overpotential for both HER and OER still greatly hinders the application of water electrolysis on a larger scale.[6,7]

Although platinum (Pt)-based materials have become the benchmark electrocatalysts for HER, the low reserves, poor stability, and high cost of Pt impede their further advancement.[8,9] Benefiting from its strong corrosion resistance and Pt-like hydrogen bond strength (65 kcal mol^{-1}), metallic ruthenium (Ru) has drawn wide attention as a HER catalyst.[10,11] However, the bonding strength of Ru with hydrogen is too strong and proper strategies for the performance improvement are still required to boost the HER activity of Ru-based electrocatalysts and close the gap with commercial Pt/C.

The HER activity of Ru-based electrocatalysts can be tuned by morphology regulation, such as designing the Ru-based nanoclusters,[12] nanoparticles,[13] nanosheets,[14] and nanotubes,[15] which can provide a large specific surface area and expose more active sites. Specifically, Ru-based materials in the form of nanoclusters can significantly boost the activity due to the increase in undercoordinated atoms.[16] Carbon-based or metallic supports are usually used to enhance the conductive property of the electrocatalyst and lower the electron transfer resistance to achieve higher HER activity.[17,18] Moreover, electronic structure modification by introducing non-metallic elements with high electronegativity or regulating the distance between the Ru d-band centers and the Fermi level, would be another effective approach to improve the HER performance.[19,20] Therefore, rational design of Ru-based electrocatalysts using morphology regulation, conductivity property control and electronic structure modification at the same time is expected to greatly lower the overpotential and yield excellent performance toward HER.

In this work, we report the design and fabrication of an efficient electrocatalyst of sub-2 nm Ru nanoclusters supported on N/S co-doped macroporous carbon spheres by a space-confined pyrolysis method with colloid spheres as the template. The unique catalyst design possesses following features. First, the macroporous carbon spheres as supports can not only provide increased specific surface area, but also offer convenient and fast mass transport channels. Second, the ultrafine Ru nanoclusters enable the exposure of more active reaction sites. Third, the N/S co-doping carbon strategy can trigger the regulation of the electronic structure in Ru atoms, further boosting the HER activity. As expected, the optimized Ru/H–S,N–C catalyst yields excellent HER activity with an overpotential of 32 mV at 10 mA cm^{-2}, a Tafel slope of 24 mV

Shanghai Key Laboratory of Special Artificial Microstructure Materials and Technology, School of Physics Science and Engineering, Tongji University, Shanghai 200092, P. R. China. E-mail: cwcheng@tongji.edu.cn

† Electronic supplementary information (ESI) available. See DOI: 10.1039/d1na00424g

dec^{-1}, and outstanding stability for more than 10 000 cycles in alkaline medium, a performance superior to those of its counterparts and commercial Pt/C catalysts.

2. Experimental section

2.1 Synthesis of Ru/H–S,N–C

In a typical process, $C_6H_{13}NO_5 \cdot HCl$ (200 mg), $RuCl_3 \cdot xH_2O$ (20 mg), and CH_4N_2S (60 mg) were dissolved in 5 mL of SiO_2 microsphere (average diameter of 227 nm) emulsion (5% W/V) and uniformly mixed first by magnetic stirring and then by ultrasonication for 2 h. The clear solution was transferred to an 80 °C oil bath pan for solvent evaporation and the self-assembly of SiO_2 opals. Then, the obtained solid powder was annealed at 900 °C for 2 h with a heating rate of 10 °C min^{-1}. The annealed products were immersed in aqueous HF (10%) for 24 h to thoroughly remove the silicon sphere templates. After drying at 80 °C overnight, the catalyst was obtained and denoted as Ru/H–S,N–C. The yield of Ru/H–S,N–C was calculated to be 8.54%, according to Table S1.† For comparison, Ru nanoparticles supported on N-doped carbon spheres (Ru/H–N–C) and pure N-doped carbon spheres (H–S, N–C) were synthesized by similar procedures without the S source and Ru source, respectively. Ru/H–S,N–C with different void sizes were prepared by changing the diameters of the SiO_2 sphere templates. The RuO_2 nanoparticle (RuO_2 NPs) catalyst was synthesized *via* the oxidation of the ultrafine Ru nanoclusters of Ru/H–SN–C at 400 °C in air for 1 h.

2.2 Characterizations

The crystal phase of the as-synthesized catalysts was analyzed on an X-ray diffraction (XRD) spectrometer (D8-Advance, Bruker Miller) with a Cu Kα radiation source ($\lambda = 1.5406$ Å). Scanning electron microscopy (SEM, FEI Sirion 200) and transmission electron microscopy (TEM, JEOL 2100 F) were utilized to observe the morphology and microstructure, respectively. The surface electronic states of the catalysts were characterized by X-ray photoelectron spectroscopy (XPS, Kratos Axis Ultra DLD). The specific surface area was examined through nitrogen adsorption isotherms using a BJBUILDER SSA-7000 adsorption analyzer at 77 K.

2.3 Electrochemical characterization

All the electrochemical measurements were carried out using an electrochemical workstation (CHI 760D) with a standard three-electrode system. 1.0 M KOH was used as the alkaline electrolyte. Catalyst-loaded glassy carbon with a diameter of 3 mm (area = 0.0707 cm^2) was utilized as the working electrode, and Hg/HgO and a graphite rod were used as the reference electrode and counter electrode, respectively. The Hg/HgO electrode was calibrated to the reversible hydrogen electrode (RHE) following the equation E (RHE) = E (Hg/HgO) + 0.91 V. To prepare the working electrode, the catalyst ink was prepared by dispersing 5 mg of sample into 1 mL of a mixture containing deionized water, ethanol, and Nafion (5% wt) at a volume ratio of 4 : 1 : 0.175. 5 mL of ink was taken and dropped vertically onto the glassy carbon electrode with a loading of 0.35 mg cm^{-2}. All data based on linear sweep voltammetry was obtained at a scan rate of 5 mV s^{-1} and was compensated for the 90% internal resistance (iR) drop. Overall water splitting measurements were conducted based on a standard two-electrode configuration with Ru/H–S,N–C as the cathode and RuO_2 NPs as the anode. The electrochemical impedance tests were carried out in the frequency range of 10^{-2} to 10^5 Hz.

3. Results and discussion

Ru/H–S,N–C was prepared through a space-confined pyrolysis procedure, as illustrated in Fig. 1. First, the solvent evaporation-induced self-assembly process was conducted in an oil bath with a mixed solution of D-glucosamine hydrochloride, thiourea, and ruthenium(III) chloride hydrate in the gaps of colloid SiO_2 opals. Then, the product was converted to Ru anchored on N- and S-co-doped carbon coated on the SiO_2 opals through annealing in an Ar atmosphere. Finally, the SiO_2 opal template was removed by etching with hydrofluoric acid solution and the Ru/H–S,N–C catalyst was obtained. For comparison, Ru nanoparticles on N-doped carbon (Ru/H–N–C) were synthesized through a similar process without the addition of thiourea. The SEM and TEM images in Fig. 2a, b and e, f show that Ru/H–S,N–C and Ru/H–N–C possess ordered macroporous structures with an average pore diameter of ~220 nm formed by the assistance of the SiO_2 template. The macroporous carbon spheres provide large specific surface area and fast mass transfer channels in HER reactions. Compared in Fig. 2b and f, in the presence of S, the diameter of the Ru nanoclusters in Ru/H–S,N–C was distributed in a range of ~1–3 nm (inset of Fig. 2b). The counted average diameter over 100 clusters was ~2 nm, which was smaller and more uniform than the diameters of the Ru nanoparticles (~8.8 nm) in Ru/H–N–C. These results suggest that the introduction of N/S atoms in carbon is beneficial to forming more nucleation sites and accelerating the nucleation rates of metallic Ru, thus minimizing the sizes and guiding a conformal distribution of Ru nanoclusters.[21–23] Smaller sized nanoclusters beneficially expose more active sites to enhance the HER performance.[12,24] The results are consistent with the TEM images in Fig. 2c and g. The HRTEM images of Ru/H–S,N–C (Fig. 2d) and Ru/H–N–C (Fig. 2h) show a measured lattice spacing of 0.23 nm, which is attributed to the Ru (100) crystal planes. The TEM-energy-dispersive X-ray spectroscopy (EDX) element mapping in Fig. 2i–m exhibits the uniform distribution of C, Ru, S, and N. The content of metallic Ru was measured to be 17.1 wt% by inductively coupled plasma atom emission spectrometry (ICP-AES) analysis, which is consistent with the 16.8 wt% extracted from the element mapping of TEM in Table S2.†

The crystal phases of Ru in Ru/H–S,N–C and Ru/H–N–C were characterized by X-ray diffraction spectrometry. In Fig. 3a, the observed peaks at 38°, 42°, 44°, 58°, 69°, 78°, and 84° belong to hexagonal Ru (PCPDF No. 89-4903).[25,26] X-ray photoelectron spectroscopy was used to characterize the elemental components and behaviors of the chemical state of Ru/H–S,N–C. For comparison, Ru/H–N–C without S and H–S,

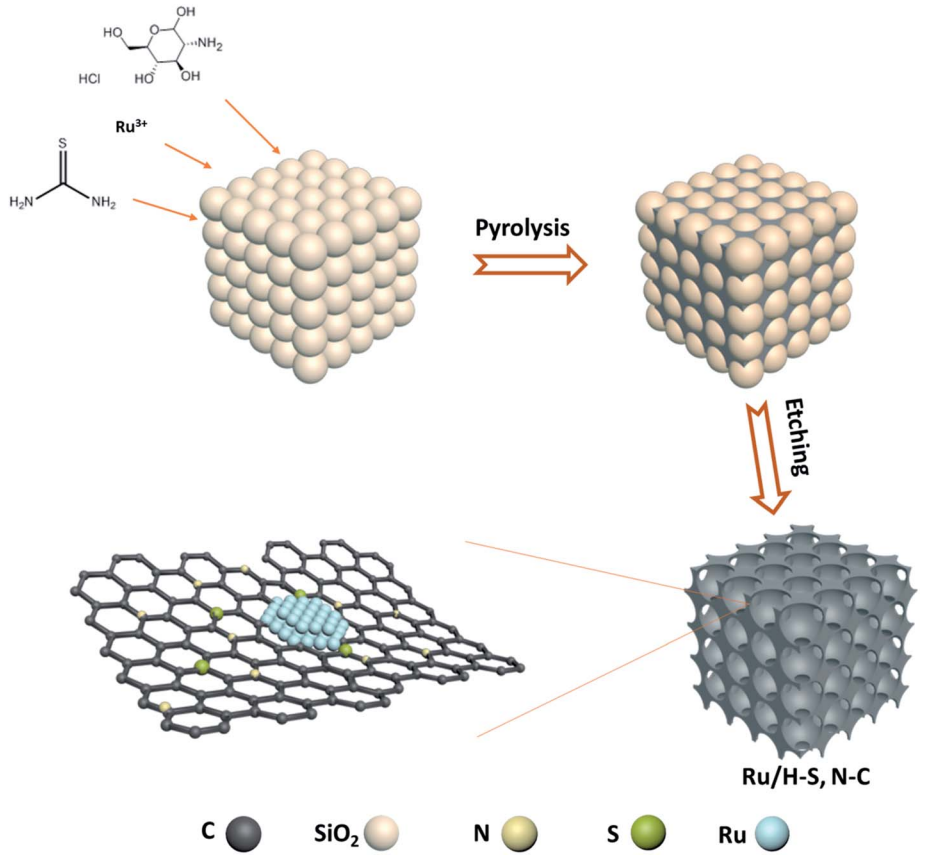

Fig. 1 An illustration of the preparation of Ru/H–S,N–C catalyst.

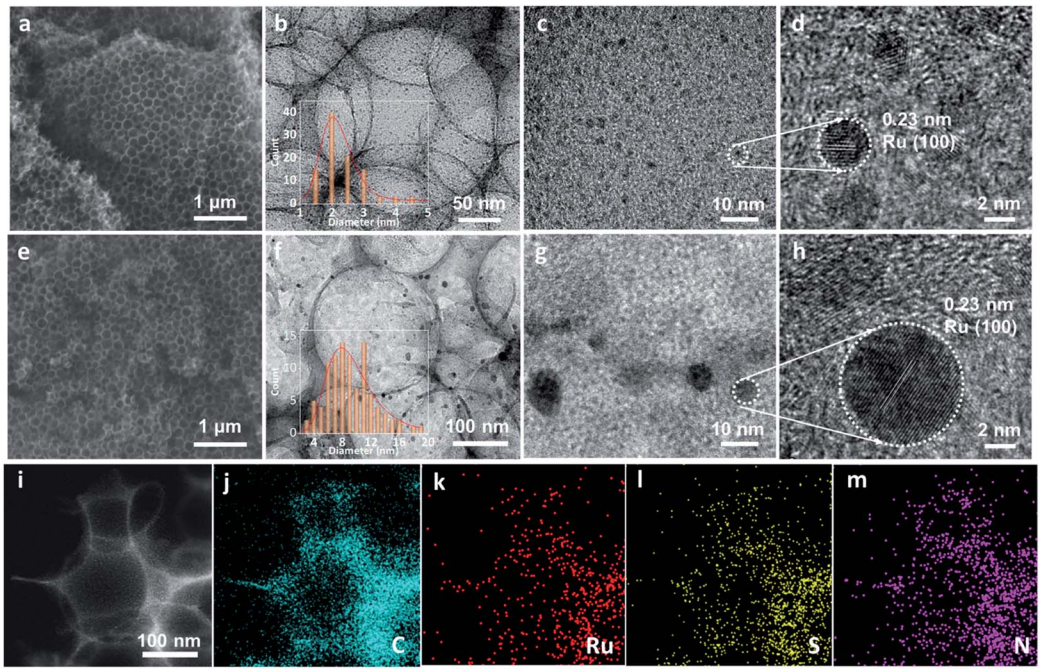

Fig. 2 Characterizations of Ru/H–S,N–C: (a) SEM, (b) TEM (inset: diameter distribution of Ru nanoclusters in Ru/H–S,N–C), and (c and d) HRTEM images; Ru/H–N–C: (e) SEM, (f) TEM (inset: diameter distribution of Ru nanoclusters in Ru/H–N–C), and (g and h) HRTEM images; (i–m) TEM-EDX element mappings of Ru/H–S,N–C.

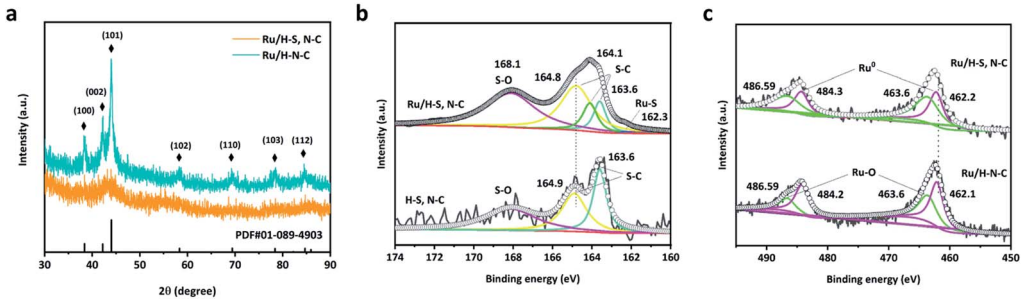

Fig. 3 (a) XRD patterns of Ru/H–S,N–C and Ru/H–N–C, (b) XPS high resolution S 2P spectra for Ru/H–S,N–C and H–S, N–C, and (c) XPS high Ru 3P resolution spectra for Ru/H–S,N–C and Ru/H–N–C.

N–C without Ru were also studied. As shown in Fig. S1,† Ru/H–S,N–C is composed of Ru, S, N, C and O without impurities. In the S 2p spectrum of Ru/H–S,N–C, despite the low S content, the Ru–S bond was directly observed at a binding energy of 162.3 eV, as shown in Fig. 3b.[27] Furthermore, a small negative shift of 0.1 eV occurred from 164.8 eV for S–C in Ru/H–S,N–C to 164.9 eV for S–C in H–S, N–C.[28] This negative shift suggested that S atoms are doped into the carbon and possess negative charge. In Fig. 3c, the Ru 3p spectrum in Ru/H–S,N–C was divided into the Ru–O bond (486.59 and 463.6 eV) and Ru^0 (484.3 and 462.2 eV).[29,30] The existence of Ru–O bonds may result from inevitable surface oxidation. For Ru^0, a small positive shift of 0.1 eV can be observed from 462.2 eV in Ru/H–S,N–C to 462.1 eV in Ru/H–N–C, which shows that Ru loses electrons and possesses positive charge, indicating electron transfer from Ru to S.[29] The C 1s spectrum in Fig. S1b† can be divided into C–C, C=C, and C=N/C=O, suggesting the formation of nitrogen-doped carbon. The Ru 3d peaks at 284.8 eV and 280.7 eV are assigned to Ru $3d_{3/2}$ and Ru $3d_{5/2}$, respectively. In Fig. S1c,† the N 1s spectrum can be deconvoluted to pyridinic N (398.2 eV), pyrrolic N (400.8 eV), graphitic N (400.0 eV), and oxidized N (402.3 eV).[8,25,31,32]

The HER performances of the as-prepared samples were evaluated in alkaline media (1.0 M KOH). In Fig. 4a, Ru/H–S,N–C shows excellent HER performance, only requiring an ultralow overpotential of 32 mV to reach 10 mA cm^{-2}, which is superior to the commercial Pt/C catalyst (η_{10} = 40 mV) and the Ru/H–N–C counterpart (η_{10} = 64 mV). The HER performance of Ru/H–S,N–C is significantly better than that of H–S, N–C, proving that the Ru nanoclusters act as the major active sites for HER. The LSV curves of Ru/H–S,N–C before and after *iR* correction are shown in Fig. S2.† Furthermore, in Fig. 4b, the Tafel slope of Ru/H–S,N–C fitted based on the polarization curve is 24 mV dec^{-1}, which is much smaller than those of Ru/H–N–C (45 mV dec^{-1}) and commercial Pt/C (42 mV dec^{-1}). These results prove that the HER process of Ru/H–S,N–C proceeds by the Volmer–Tafel mechanism and that sulfur doping in Ru/H–S,N–C significantly enhances the reaction kinetics towards HER. Fig. 4c and Table S3† summarize the key parameters in HER performance of recently reported Ru-based catalysts with

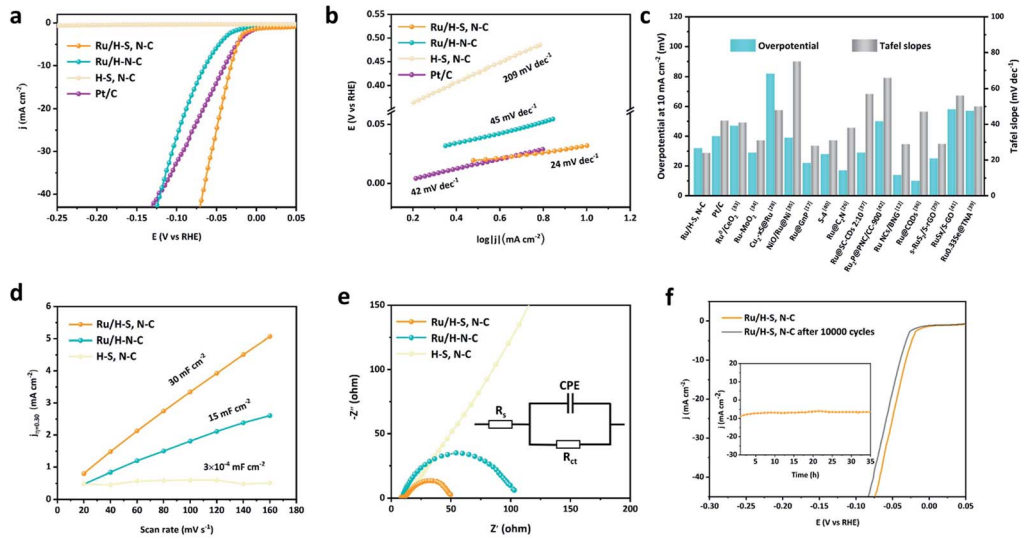

Fig. 4 (a and b) LSV curves and Tafel slopes of Ru/H–S,N–C, Ru/H–N–C, and Pt/C, (c) comparison chart of overpotentials at 10 mA cm^{-2} and Tafel slopes for Ru/H–S,N–C, Pt/C, and recently reported Ru-based catalysts,[12,17,26,29,33–42] (d and e) C_{dl} and EIS (inset: equivalent circuits from fitting the related Nyquist curves) of Ru/H–S,N–C and Ru/H–N–C, (f) ADT test (inset: *i*–*t* curve of Ru/H–SN–C).

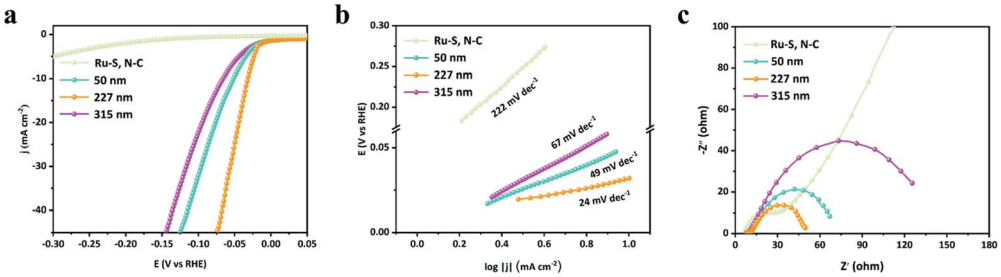

Fig. 5 (a–c) LSV curves, Tafel slopes, and EIS of Ru/H–S,N–C with different pore diameters and Ru–S, N–C without pores.

commercial Pt/C for comparison.[12,17,26,29,33–42] Among Pt/C and the various Ru-based catalysts, Ru/H–S,N–C exhibits relatively higher HER activity.

To elucidate the electrochemical behavior of Ru/H–N–C, H–S, N–C, and Ru/H–S,N–C, electrochemical double-layer capacitance (C_{dl}) with positive correction to the electrochemical active surface area (ECSA) was performed. In Fig. 4d, the C_{dl} of Ru/H–S,N–C calculated based on cyclic voltammetry (Fig. S3†) is 30 mF cm^{-2}, which is twice that of Ru/H–N–C (15 mF cm^{-2}) and far greater than that of H–S, N–C. The larger ECSA of Ru/H–S,N–C is mainly due to the formation of ultrafine Ru nanoclusters which provide more exposed Ru sites accessible to the electrolyte in HER, leading to excellent HER performance.[27,43,44] Furthermore, electrochemical impedance spectroscopy (EIS) is used to discover the influence of conductivity property control on HER performance by measuring electron-transfer resistance (R_{ct}) at the interface between catalyst and electrolyte. In Fig. 4e, Ru/H–S,N–C has the smallest R_{ct} compared with Ru/H–N–C and H–S, N–C, showing the fastest electron transport and reaction kinetics.[45–49] The macroporous hollow S,N-doped carbon spheres not only provide good conductivity, but also facilitate electrolyte penetration to accelerate mass transfer during HER. Therefore, the excellent HER performance of Ru/H–S,N–C can be attributed to both the number of exposed active sites and fast mass/electron transport.

The durability of Ru/H–S,N–C was explored using the accelerated durability test (ADT) and *i–t* curves.[4,26,50] In Fig. 4f, after 10 000 cycles of cyclic voltammetry, the overpotential at 10 mA

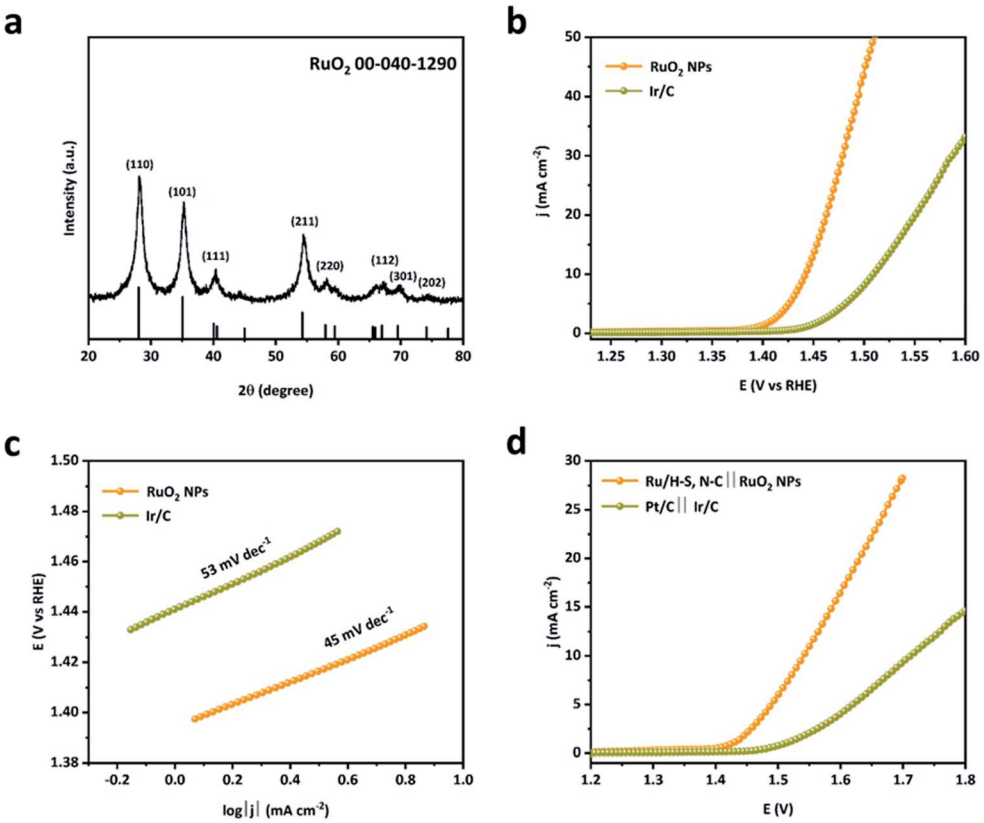

Fig. 6 (a) XRD pattern of RuO_2 NPs, (b and c) LSV curves and Tafel slopes of RuO_2 NPs and Ir/C for OER, and (d) polarization curves of Ru/H–S, N–C||RuO_2 NPs and Pt/C||Ir/C for overall water splitting.

cm^{-2} of Ru/H–S,N–C increased only 7 mV. Seen in the inset plots in Fig. 4f, the small decay in current density in the *i–t* curves after 35 h of operation shows good durability as well. After the durability test, the uniform macroporous structure and crystal plane showed no obvious change, as can be seen in Fig. S4.† From the XPS characterization in Fig. S5,† the chemical composition and surface electronic structure of Ru/H–S,N–C are also unchanged after the stability test. In addition, the Ru content was scarcely changed, as shown in Table S4,† as the atomic ratio of Ru 3p to N 1s was calculated to be 0.302 before the stability test and 0.305 after the stability test.

In order to investigate the effect of pore sizes on HER performance, Ru/H–S,N–C-n (n represents the diameter of the SiO_2 template) with different SiO_2 template diameters were prepared, including 50, 227, and 315 nm, as well as Ru–S, N–C without a SiO_2 template. In Fig. 5a and b, the Ru/H–S,N–C-227 shows the smallest overpotential at 10 mA cm^{-2} and Tafel slope compared to those of Ru/H–S,N–C-50 ($\eta_{10} = 52$ mV, $b = 49$ mV dec^{-1}), Ru/H–S,N–C-315 ($\eta_{10} = 66$ mV, $b = 67$ mV dec^{-1}), and Ru–S, N–C, indicating that Ru/H–S,N–C-227 possesses the highest HER activity. The optimal HER activity of Ru/H–S, N–C-227 comes from the optimization of the specific surface area and charge transfer process. Although the BET specific area values follow the order of Ru/H–S,N–C-50 > Ru/H–S,N–C-227 > Ru/H–S,N–C-315 > Ru–S, N–C (Fig. S6†),[51] in Fig. 5c, the EIS plots of the four samples show that Ru/H–S,N–C-227 possessed the smallest charge transfer resistance, leading to faster charge transportation at the interface of Ru and N,S-co-doped macroporous carbon.

To evaluate their prospect of practical application in overall water splitting devices, RuO_2 NPs were obtained *via* the one-step oxidation of Ru/H–S,N–C-227 samples by annealing at 400 °C in air for 1 h and were used as an OER catalyst. In Fig. 6a, the XRD pattern of RuO_2 NPs matches well with that of RuO_2 (PCPDF no. 040-1290),[52] indicating that metallic Ru is successfully converted into RuO_2. In Fig. 6b–c, benefiting from S,N-co-doped macroporous carbon as a carrier, RuO_2 NPs need an overpotential of only 210 mV to achieve 10 mA cm^{-2}, superior to the commercial 20% Ir/C (280 mV), and possess the smallest Tafel slope of 45 mV dec^{-1} in alkaline media. Furthermore, when used as an overall water splitting device, Ru/H–S,N–C‖RuO_2 NPs comprised of Ru/H–S,N–C-227 for HER and RuO_2 NPs for OER shows a cell voltage of 1.54 V at 10 mA cm^{-2}, which is much lower than that of the commercial Pt/C‖Ir/C (1.71 V), as seen in Fig. 6d. These results show the probability of replacing commercial Pt/C catalysts with Ru-based electrocatalysts in industrial water electrolysis.

4. Conclusions

In summary, we have developed ultrafine Ru nanoclusters (~2 nm) supported on N/S-co-doped macroporous carbon spheres as an efficient catalyst with excellent HER performance. Macroporous carbon spheres as supports ensure a large specific surface area and fast mass transfer channels. The introduction of sulfur and nitrogen atoms in the carbon supports reduces the size of Ru nanoclusters for higher exposure of active sites and regulates the electronic structure of Ru, leading to significantly improved HER performance. Combining all the merits above, the Ru/H–S,N–C-227 catalyst exhibits the highest HER activity with an overpotential of 32 mV at 10 mA cm^{-2}, a Tafel slope of 24 mV dec^{-1}, and good stability, outperforming the reference samples of Ru/H–N–C-227 and commercial Pt/C.

Author contributions

Yijie Wang: methodology, validation, formal analysis, writing – review & editing. Wenjie Luo: methodology, writing – original draft, investigation. Haojie Li: methodology, visualization, writing – review & editing. Chuanwei Cheng: conceptualization, funding acquisition, project administration, resources, writing – review & editing.

Conflicts of interest

There are no conflicts to declare.

Acknowledgements

We acknowledge the financial support by the National Natural Science Foundation of China (Grant No. 51772213), Shanghai Science and Technology Committee (Grant No. 18ZR1442300 and 18JC1410900) and Shanghai Key Laboratory of Special Artificial Microstructure Materials and Technology.

References

1 M. S. Faber and S. Jin, *Energy Environ. Sci.*, 2014, **7**, 3519–3542.
2 F. Dawood, M. Anda and G. M. Shafiullah, *Int. J. Hydrogen Energy*, 2020, **45**, 3847–3869.
3 S. Sharma, S. Basu, N. P. Shetti and T. M. Aminabhavi, *Sci. Total Environ.*, 2020, **713**, 136633.
4 H.-C. Fu, P. Varadhan, M.-L. Tsai, W. Li, Q. Ding, C.-H. Lin, M. Bonifazi, A. Fratalocchi, S. Jin and J.-H. He, *Nano Energy*, 2020, **70**, 104478.
5 Y. Ma, Z. Guo, X. Dong, Y. Wang and Y. Xia, *Angew. Chem., Int. Ed.*, 2019, **58**, 4622–4626.
6 R. Ge, S. Wang, J. Su, Y. Dong, Y. Lin, Q. Zhang and L. Chen, *Nanoscale*, 2018, **10**, 13930–13935.
7 J. Wang, Z. Wei, S. Mao, H. Li and Y. Wang, *Energy Environ. Sci.*, 2018, **11**, 800–806.
8 S. Yuan, Z. Pu, H. Zhou, J. Yu, I. S. Amiinu, J. Zhu, Q. Liang, J. Yang, D. He, Z. Hu, G. Van Tendeloo and S. Mu, *Nano Energy*, 2019, **59**, 472–480.
9 Q. Ju, R. Ma, Y. Pei, B. Guo, Z. Li, Q. Liu, T. Thomas, M. Yang, G. J. Hutchings and J. Wang, *Adv. Energy Mater.*, 2020, **10**, 2000067.
10 J. Yu, Q. He, G. Yang, W. Zhou, Z. Shao and M. Ni, *ACS Catal.*, 2019, **9**, 9973–10011.
11 S.-Y. Bae, J. Mahmood, I.-Y. Jeon and J.-B. Baek, *Nanoscale Horiz.*, 2020, **5**, 43–56.

12 S. Ye, F. Luo, T. Xu, P. Zhang, H. Shi, S. Qin, J. Wu, C. He, X. Ouyang, Q. Zhang, J. Liu and X. Sun, *Nano Energy*, 2020, **68**, 104301.
13 Q.-Q. Chen, X. Yang, C.-C. Hou, K. Li and Y. Chen, *J. Mater. Chem. A*, 2019, **7**, 11062–11068.
14 X. Kong, K. Xu, C. Zhang, J. Dai, S. Norooz Oliaee, L. Li, X. Zeng, C. Wu and Z. Peng, *ACS Catal.*, 2016, **6**, 1487–1492.
15 Q. Lu, A.-L. Wang, H. Cheng, Y. Gong, Q. Yun, N. Yang, B. Li, B. Chen, Q. Zhang, Y. Zong, L. Gu and H. Zhang, *Small*, 2018, **14**, 1801090.
16 C. Li and J. B. Baek, *ACS Omega*, 2020, **5**, 31–40.
17 F. Li, G.-F. Han, H.-J. Noh, I. Ahmad, I.-Y. Jeon and J.-B. Baek, *Adv. Mater.*, 2018, **30**, 1803676.
18 S. Li, R. Ma, Y. Pei, B. Mao, H. Lu, M. Yang, T. Thomas, D. Liu and J. Wang, *J. Phys. Chem. Lett.*, 2020, **11**, 3436–3442.
19 W. Luo, Y. Wang and C. Cheng, *Mater. Today Phys.*, 2020, **15**, 100274.
20 Y. Liu, X. Li, Q. Zhang, W. Li, Y. Xie, H. Liu, L. Shang, Z. Liu, Z. Chen, L. Gu, Z. Tang, T. Zhang and S. Lu, *Angew. Chem., Int. Ed.*, 2020, **59**, 1718–1726.
21 M. Xia, W. Ding, K. Xiong, L. Li, X. Qi, S. Chen, B. Hu and Z. Wei, *J. Phys. Chem. C*, 2013, **117**, 10581–10588.
22 F. Yang, X. Bao, Y. Zhao, X. Wang, G. Cheng and W. Luo, *J. Mater. Chem. A*, 2019, **7**, 10936–10941.
23 X. Sun, X. Gao, J. Chen, X. Wang, H. Chang, B. Li, D. Song, J. Li, H. Li and N. Wang, *ACS Appl. Mater. Interfaces*, 2020, **12**, 48591–48597.
24 M. An, L. Du, C. Du, Y. Sun, Y. Wang, G. Yin and Y. Gao, *Electrochim. Acta*, 2018, **285**, 202–213.
25 W. Li, Y. Liu, M. Wu, X. Feng, S. A. T. Redfern, Y. Shang, X. Yong, T. Feng, K. Wu, Z. Liu, B. Li, Z. Chen, J. S. Tse, S. Lu and B. Yang, *Adv. Mater.*, 2018, **30**, 1800676.
26 J. Mahmood, F. Li, S. M. Jung, M. S. Okyay, I. Ahmad, S. J. Kim, N. Park, H. Y. Jeong and J. B. Baek, *Nat. Nanotechnol.*, 2017, **12**, 441–446.
27 V. Ramalingam, P. Varadhan, H. C. Fu, H. Kim, D. Zhang, S. Chen, L. Song, D. Ma, Y. Wang, H. N. Alshareef and J. H. He, *Adv. Mater.*, 2019, **31**, e1903841.
28 D. Luo, B. Zhou, Z. Li, X. Qin, Y. Wen, D. Shi, Q. Lu, M. Yang, H. Zhou and Y. Liu, *J. Mater. Chem. A*, 2018, **6**, 2311–2317.
29 J. Yu, Y. Guo, S. Miao, M. Ni, W. Zhou and Z. Shao, *ACS Appl. Mater. Interfaces*, 2018, **10**, 34098–34107.
30 W. Fang, H. Hu, T. Jiang, G. Li and M. Wu, *Carbon*, 2019, **146**, 476–485.
31 J. Yu, G. Li, H. Liu, L. Zhao, A. Wang, Z. Liu, H. Li, H. Liu, Y. Hu and W. Zhou, *Adv. Funct. Mater.*, 2019, **29**, 1901154.
32 J. N. Tiwari, A. M. Harzandi, M. Ha, S. Sultan, C. W. Myung, H. J. Park, D. Y. Kim, P. Thangavel, A. N. Singh, P. Sharma, S. S. Chandrasekaran, F. Salehnia, J. W. Jang, H. S. Shin, Z. Lee and K. S. Kim, *Adv. Energy Mater.*, 2019, **9**, 1900931.
33 E. Demir, S. Akbayrak, A. M. Onal and S. Ozkar, *ACS Appl. Mater. Interfaces*, 2018, **10**, 6299–6308.
34 P. Jiang, Y. Yang, R. Shi, G. Xia, J. Chen, J. Su and Q. Chen, *J. Mater. Chem. A*, 2017, **5**, 5475–5485.
35 C. Zhong, Q. Zhou, S. Li, L. Cao, J. Li, Z. Shen, H. Ma, J. Liu, M. Lu and H. Zhang, *J. Mater. Chem. A*, 2019, **7**, 2344–2350.
36 W. D. Li, Z. H. Wei, B. Y. Wang, Y. Liu, H. Q. Song, Z. Y. Tang, B. Yang and S. Y. Lu, *Mater. Chem. Front.*, 2020, **4**, 277–284.
37 Y. Liu, Y. Yang, Z. Peng, Z. Liu, Z. Chen, L. Shang, S. Lu and T. Zhang, *Nano Energy*, 2019, **65**, 104023.
38 D. Yoon, J. Lee, B. Seo, B. Kim, H. Baik, S. H. Joo and K. Lee, *Small*, 2017, **13**, 1700052.
39 K. Wang, Q. Chen, Y. Hu, W. Wei, S. Wang, Q. Shen and P. Qu, *Small*, 2018, **14**, e1802132.
40 J. Su, Y. Yang, G. Xia, J. Chen, P. Jiang and Q. Chen, *Nat. Commun.*, 2017, **8**, 14969.
41 P. Li, X. Duan, S. Wang, L. Zheng, Y. Li, H. Duan, Y. Kuang and X. Sun, *Small*, 2019, **15**, e1904043.
42 T. Liu, B. Feng, X. Wu, Y. Niu, W. Hu and C. M. Li, *ACS Appl. Energy Mater.*, 2018, **1**, 3143–3150.
43 H. Zhang, Z. Ma, J. Duan, H. Liu, G. Liu, T. Wang, K. Chang, M. Li, L. Shi, X. Meng, K. Wu and J. Ye, *ACS Nano*, 2016, **10**, 684–694.
44 T. Qiu, Z. Liang, W. Guo, S. Gao, C. Qu, H. Tabassum, H. Zhang, B. Zhu, R. Zou and Y. Shao-Horn, *Nano Energy*, 2019, **58**, 1–10.
45 M. Li, H. Wang, W. Zhu, W. Li, C. Wang and X. Lu, *Adv. Sci.*, 2020, **7**, 1901833.
46 Q. Qin, H. Jang, L. Chen, G. Nam, X. Liu and J. Cho, *Adv. Energy Mater.*, 2018, **8**, 1801478.
47 B. Lu, L. Guo, F. Wu, Y. Peng, J. E. Lu, T. J. Smart, N. Wang, Y. Z. Finfrock, D. Morris, P. Zhang, N. Li, P. Gao, Y. Ping and S. Chen, *Nat. Commun.*, 2019, **10**, 631.
48 N. K. Oh, C. Kim, J. Lee, O. Kwon, Y. Choi, G. Y. Jung, H. Y. Lim, S. K. Kwak, G. Kim and H. Park, *Nat. Commun.*, 2019, **10**, 1723.
49 Z. Peng, H. Wang, L. Zhou, Y. Wang, J. Gao, G. Liu, S. A. T. Redfern, X. Feng, S. Lu, B. Li and Z. Liu, *J. Mater. Chem. A*, 2019, **7**, 6676–6685.
50 L. Zhang, R. Si, H. Liu, N. Chen, Q. Wang, K. Adair, Z. Wang, J. Chen, Z. Song, J. Li, M. N. Banis, R. Li, T. K. Sham, M. Gu, L. M. Liu, G. A. Botton and X. Sun, *Nat. Commun.*, 2019, **10**, 4936.
51 F. Li, X. Zhao, J. Mahmood, M. S. Okyay, S. M. Jung, I. Ahmad, S. J. Kim, G. F. Han, N. Park and J. B. Baek, *ACS Nano*, 2017, **11**, 7527–7533.
52 C.-Z. Yuan, Y.-F. Jiang, Z.-W. Zhao, S.-J. Zhao, X. Zhou, T.-Y. Cheang and A.-W. Xu, *ACS Sustainable Chem. Eng.*, 2018, **6**, 11529–11535.